Published in Journal of Applied Physics 93, issue 9, 5727-5731, 2003
which should be used for any reference to this work


# Microstructure and open-circuit voltage of $n-i-p$ microcrystalline silicon solar cells

J. Bailat,[a] E. Vallat-Sauvain, L. Feitknecht, C. Droz, and A. Shah
*Institut de Microtechnique, Université de Neuchâtel, Rue Breguet 2, CH-2000 Neuchâtel, Switzerland*

A series of microcrystalline silicon $n-i-p$ solar cells has been deposited by very high frequency plasma enhanced chemical vapor deposition at various values of silane to hydrogen source gas ratio and on two different substrate types. Relationships between microstructure and electrical characteristics of these solar cells are investigated by transmission electron microscopy, atomic force microscopy, and $I(V)$ measurements. A mixed phase (so-called heterophase) layer consisting of amorphous plus microcrystalline material is observed at the bottom of the solar cell and identified here as one of the key microstructural features of the device: the relationship between the crystalline nuclei density and the heterophase layer thickness is presented as well as its relationship with the open-circuit voltage ($V_{oc}$). The effects of substrate roughness and of silane to hydrogen gas ratio used for the fabrication of the device on the heterophase layer are evidenced. These observations underline the importance of the first stages of growth of the intrinsic ($i$) layer for the fabrication of high- $V_{oc}$ $n-i-p$ microcrystalline solar cells.

## I. INTRODUCTION

Microcrystalline silicon ($\mu c-$Si:H) is a promising material for thin-film ($<10\,\mu$m) solar cell applications.[1] This material is commonly prepared with a plasma enhanced chemical vapor deposition (PECVD) process using silane diluted with hydrogen in the plasma gas phase. Microcrystalline silicon is not a unique, well-defined material but a complex mixture of amorphous and nanocrystalline silicon plus grain boundaries.[2] The respective amorphous/microcrystalline volume fraction depend mostly on the silane concentration ($SC=[SiH_4]/[SiH_4+H_2]$) used for the deposition of the material. Despite the complexity in material microstructure, performant photovoltaic cells have already been fabricated, with electrical conversion efficiencies over 9%.[3–5] Currently the best devices are obtained with $i$ layers prepared under conditions close to the amorphous/microcrystalline transition, and thus SC is an important parameter for device optimization.[5–7] Furthermore, the substrate, on which deposition takes place, plays a critical role on microcrystalline growth,[8–11] particularly at deposition conditions close to the amorphous/microcrystalline transition. Under these deposition conditions, the thickness evolution of the material crystallinity also exhibits a transition from amorphous to microcrystalline within the range 0.5 – 1.5 $\mu$m.[8] However, an open question that remains is to which extent the material microstructure influences the electrical characteristics of the device. For this study, the material as incorporated into the active device has been characterized with atomic force microscopy (AFM), transmission electron microscopy (TEM) and x-ray diffraction (XRD). These characterization techniques have been applied directly to two dilution series of $n-i-p$ solar cells deposited for various values of SCs. The two series were obtained by depositing the cells in the same run on two different substrates, namely, on a glass substrate with a sputtered ZnO layer and on a glass substrate with a ZnO layer fabricated by low pressure chemical vapor deposition (LPCVD).

In the series of devices studied here, in contrast with Ref. 5, the amorphous volume fraction is not homogenously distributed over the whole device thickness. Along the first hundreds of nanometers the microstructure consists of a mixture of conical conglomerates of crystallites embedded in an amorphous tissue that will be called thereafter the heterophase layer.

The density of crystalline nuclei and the height of the heterophase layer are identified here as the dominant microstructural parameters in the relationship between material microstructure and device electrical performances.

## II. EXPERIMENT

### A. Cell fabrication

Two dilution series of $n-i-p$ $\mu c-$Si:H solar cells were deposited on glass substrates coated with transparent conductive oxide (TCO) layers. A series of cells was deposited on aluminum-doped sputtered ZnO, a rather flat TCO (root-mean-square roughness of 4 nm), whereas another series was deposited on boron-doped LPCVD ZnO, which is a much rougher TCO (rms$=60$ nm). The $n-i-p$ cells were deposited in the same run on both TCOs at SC for the $i$ layer of 5%, 5.5%, 6%, 6.5%, and 7%. The other deposition parameters of the $i$ layer were a substrate temperature of 250 °C, a pressure of 0.5 mbar, a plasma excitation frequency of 130 MHz and a power of 30 W, and they were maintained constant in the whole series. Under these conditions, the thickness of the $i$ layer was approximately 2.2 $\mu$m for the cells on sputtered ZnO and 2.7 $\mu$m for the cells on LPCVD

[a]Electronic mail: julien.bailat@unine.ch

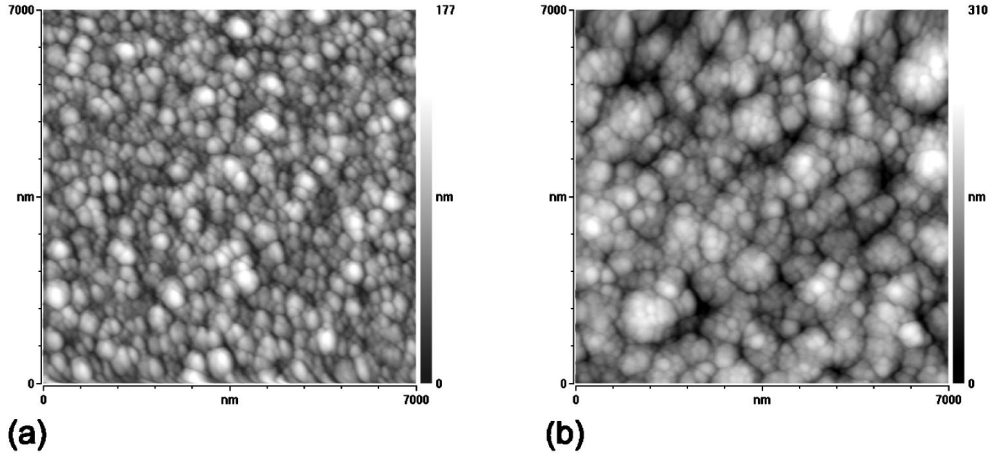


FIG. 1. (a) AFM scan of the top layer (*p* layer) of the solar cell with SC=5% on sputtered ZnO. Such topography is representative of all the cells of this series. The lateral size of the surface features, measured from the Fourier transform power spectrum of the AFM scan is 600 nm. (b) AFM scan of the top layer (*p* layer) of the solar cell deposited with SC=5% on LPCVD ZnO. This surface morphology is representative of all the cells of this series. Conglomerate lateral size, measured from the Fourier transform power spectrum of the AFM scan is in the order of 1000 nm.

ZnO. The deposition parameters of the *n* and *p* layers were the same for the whole series and were optimized in such a way as to produce highly microcrystalline material on glass.

### B. Characterization of the microstructure of the *i* layer

XRD was used on all the cells in order to evaluate the average crystallinity of the whole device. XRD was performed on a Philips PW3020 diffractometer, using the Bragg–Brentano geometry ($\vartheta-2\vartheta$ scan). An accelerating voltage of 30 kV and a current of 40 mA were used to produce Cu $K\alpha$ radiation at a wavelength of 1.5418 Å.

TEM permits to observe the microstructure of the various (ZnO, *n*, *i*, and *p*) layers within the cell. A piece of each cell (except for cells deposited at 6% SC) was prepared as a cross-section sample for TEM examination with the help of the technique described in Ref. 12. This technique consists of gluing head to tail two pieces of the sample in order to obtain a ''sandwich.'' Then, a corner with an angle between 0.6° and 0.9° is made by mechanically polishing the sandwich. The last step of this technique, a short ion milling procedure, is used only for sample cleaning. TEM observations were made on a Philips CM200 TEM microscope operated at 200 kV.

AFM was performed on the top *p* layer of the device in order to evaluate the root mean square roughness and the lateral size of the plasma-exposed growing surface features. These measurements were performed in the noncontact (tapping) mode on a Vista Burleigh Instruments scanning probe microscope.

## III. RESULTS

### A. Surface topography

In Fig. 1(a), an AFM scan of the top surface, i.e., the *p* layer, representative of all the cells deposited on sputtered ZnO is given. By comparing the AFM and TEM micrographs on the same solar cell [cf. Figs. 1(a) and 2(a)], we can conclude that conglomerates of crystallites with an average diameter of approximately 600 nm emerge at the growing surface of the *p* layer. In this dilution series, there is no major effect of SC on the surface roughness of the device, the latter is comprised between 20 and 25 nm (rms value) (Fig. 3). It is larger than the initial roughness of the TCO (rms=4 nm) and it is similar to fully microcrystalline layers of comparable thickness directly deposited on glass.[2]

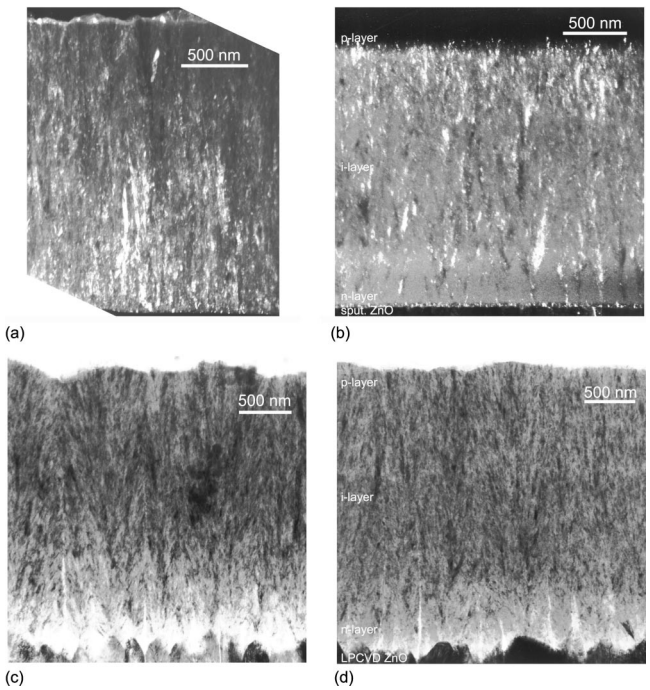


FIG. 2. TEM dark-field micrographs of the cells deposited at SC=5% and at SC=7% on flat sputtered ZnO, (a) and (b), respectively. The heterophase layer is barely visible in (a) whereas it is much larger in (b). The highly microcrystalline *n* layer clearly appears as a thin line made up of shiny dots on top of dark sputtered ZnO (b). TEM bright-field micrographs of cells deposited at SC=5% and SC=6.5% on LPCVD ZnO, (c) and (d), respectively. The amorphous phase (homogeneously gray) in the heterophase layer is clearly visible in (d). Note the conical shape of the conglomerates of grains and the enhancement of their lateral size in (c) and (d) compared to (a) and (b). AFM scans of the surface of the cells presented in (a) and (c) are shown in Fig. 1.

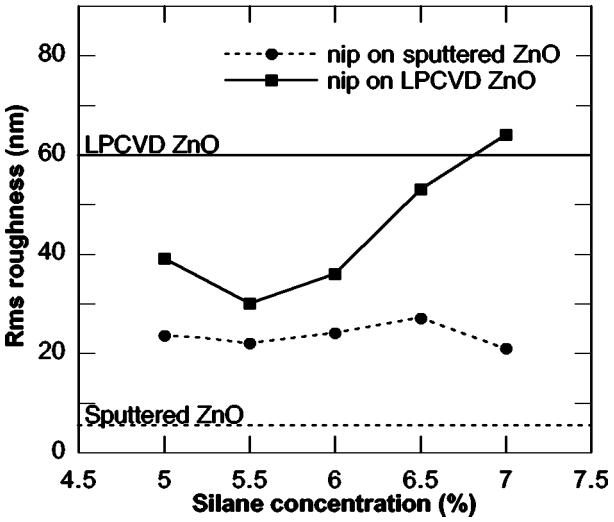


FIG. 3. Rms roughness measured on the *p* layer by AFM on both series of cells. For the cells deposited on sputtered ZnO, the top layer rms roughness is larger than the roughness of the flat substrate (straight line at bottom). On the other hand, the rms roughness of the cells deposited on the rough LPCVD ZnO surface is equal to or smaller than the initial rms roughness of the substrate.

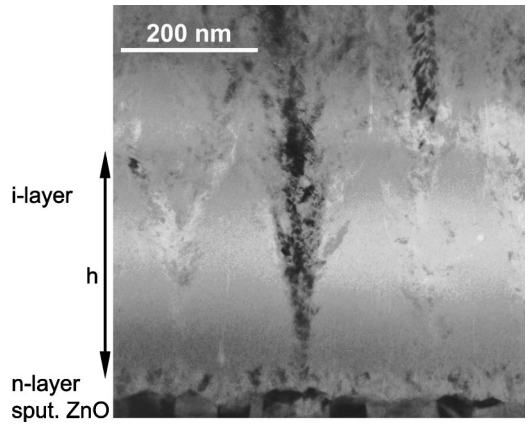


FIG. 4. TEM bright-field micrograph of the first hundreds of nanometers of an $n-i-p$ solar cell. The *i* layer was deposited with SC=7% on a highly microcrystalline *n*-layer on top of sputtered ZnO. The *i*-layer microcrystalline phase consists of conical conglomerates of nanocrystals, which are embedded in an amorphous matrix. The height at which conglomerates coalesce is defined as the thickness of the heterophase layer *h*. On this micrograph, the nucleation density $n_d$ is approximately 5 $\mu m^{-1}$.

The surface topography of cells deposited on top of LPCVD ZnO consists of cauliflower-like grains [see Fig. 1(b)]. By comparison with our TEM micrograph of the same cell [cf. Fig. 2(c)], we conclude that large conglomerates of crystallites emerge at the surface. The lateral size of the conglomerates, as evaluated from the power spectrum of the Fourier transform of the AFM micrograph, is approximately 1 $\mu$m, i.e., almost twice as much as that evaluated for microcrystalline material grown on flat sputtered ZnO. As supported by TEM micrographs (see below), the enhanced lateral size of the conglomerates in cells grown on LPCVD ZnO as compared with that of cells grown on flat sputtered ZnO can be explained in terms of competitive growth promoted by the surface roughness of the substrate. The top surface roughness of the series of cells (Fig. 3) deposited by LPCVD ZnO increases with increasing SC, from values close to those measured for the cells on sputtered ZnO towards the typical value measured for the LPCVD ZnO bare substrate (rms value of 60 nm). The evolution of top surface roughness with SC (for a given substrate) is of importance for light trapping purpose. Indeed, according to the definition and calculated values in Ref. 13 for the optical scattering factor, the latter varies notably in the range of rms roughness measured here (in Fig. 3).

### B. Bulk microstructure

A characteristic TEM micrograph of an $n-i-p$ cell deposited on sputtered ZnO is given in Fig. 4. At the bottom of the micrograph, the TCO appears dark. It consists of crystallites (average diameter of about 40 nm) emerging to the surface with well defined but short facets. On top of it, the *n* layer appears compact and strongly microcrystalline. Its thickness of about 30 nm is constant over the field of observation. On top of the *n* layer, the *i* layer exhibits a more complicated microstructure. It consists of three phases: the conical conglomerates of nanocrystals (the so-called microcrystalline phase, appearing with the whole black and white contrast on the micrograph), the amorphous phase (appearing uniformly gray on the micrograph) and finally, in some cases, cracks/voids. This mixed phase layer will thereafter be called ''heterophase layer.'' It is within this layer that the volume fraction of amorphous material is higher than within the rest of the *i* layer. Such a heterophase layer has been observed in all the solar cells presented here. Above the heterophase layer, starting at the so-called contact threshold where microcrystalline cones coalesce, microcrystalline columns grow up to the top of the solar cell (see Fig. 2). Note that the medium resolution TEM studies conducted here do not permit to quantify the volume fraction of amorphous material still present above the heterophase layer. We will, therefore, focus our study on the modifications of the heterophase layer with SC and the substrate type, that are observable modifications of the microstructure of the *i* layers in the solar cells presented here.

In the aim of describing quantitatively the evolution of the microstructure and specifically of the heterophase layer of the material incorporated in the devices, two parameters measured on TEM micrographs will be used in this paper: the linear nuclei density $n_d$ and the heterophase layer thickness *h*. The linear nuclei density is the average number of nuclei per micrometer. By definition, the inverse of $n_d$ is the mean distance between two nuclei. The heterophase layer thickness *h* (nm) is evaluated as the average thickness at which the conglomerates of crystallites coalesce, measured on a vertical line from the top of the *n* layer in $n-i-p$ solar cells.

In the series of cells deposited on sputtered ZnO, we can observe that every conglomerate starts growing from the *n* layer. Thus, this doped layer plays the role of a nucleation layer. Note that in this series (as in the next series on LPCVD ZnO), no continuous amorphous incubation layer separating the underlying (microcrystalline) doped layer and the microcrystalline *i* layer can be observed, as had been previously

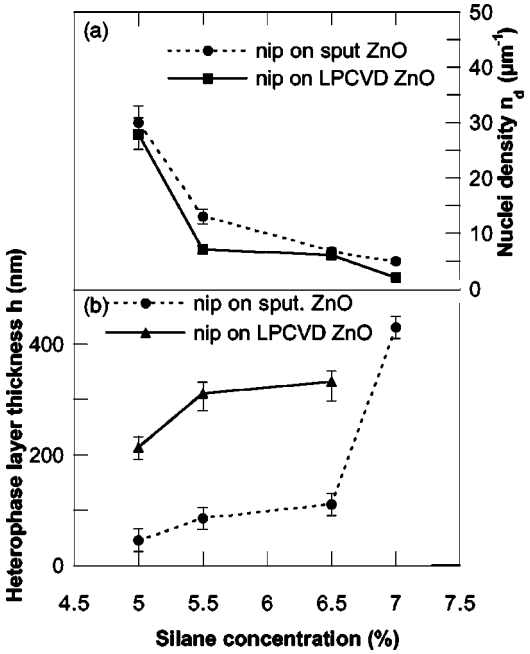


FIG. 5. (a) Evolution of linear nuclei density $n_d$ of the cells on sputtered and LPCVD ZnO as a function of silane concentration. (b) Evolution of the heterophase layer thickness on sputtered ZnO and LPCVD ZnO as a function of silane concentration. Heterophase layer thickness is significantly higher on LPCVD ZnO, as most of the material deposited in the valleys of the TCO is amorphous. Note that both $h$ and $n_d$, on both TCOs, follow the same trend versus the silane concentration.

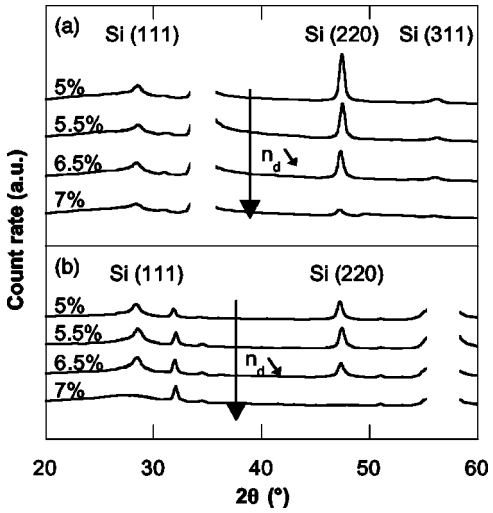


FIG. 6. (a) Raw XRD spectra of the cells on sputtered ZnO and (b) on LPCVD ZnO. Crystalline volume within the solar cell evolves as the total area under XRD (Si) peaks. The density of nuclei $n_d$ decreases when overall crystallinity decreases.

reported for $p-i-n$ solar cells.[14] High resolution TEM (HRTEM) observations of the $n-i$ interface indicate that the *i*-layer crystallites grow epitaxially on the *n*-layer grains, as already reported.[15] The mean lateral size of the nuclei of the *i* layer is of the order of the *n*-layer thickness (i.e., 30 nm) (see Fig. 4). The gap between the nuclei is filled with amorphous material. As growth proceeds, the conical conglomerates of nanocrystals coalesce and finally result in compact columnar microstructure. The influence of SC on $n_d$ and on $h$ is shown in Figs. 5(a) and 5(b). The decrease of $h$ and increase of $n_d$ are in good agreement with the overall change of crystallinity as observed on XRD spectra (Fig. 6). What these XRD spectra do not indicate is the location of the amorphous fraction, which is shown by our TEM studies to lie mostly at the bottom of the *i* layer. Note that the evaluation of the crystallite size from these XRD indicates that, in both dilution series, the average crystallite size remains within the limited range of $20\,\text{nm} \pm 4$.

On the other hand, the LPCVD ZnO coated glass substrate is a rough (rms roughness of about 60 nm) substrate consisting of regular tetrahedrons as previously described.[16] TEM micrographs of the solar cells deposited on this substrate are given in Figs. 2(c) and 2(d). As we could deduce from TEM micrograph of the cell deposited at SC=7% (shown in Ref. 10), which is almost completely amorphous (see XRD spectrum in Fig. 6), the *n* layer on LPCVD ZnO is thicker on top of the tetrahedrons than in the valleys in between and not as compact as on sputtered ZnO. On top of the *n* layer, the nucleation of *i*-layer is not homogenous over the TCO, but occurs preferentially on the upper part of the ZnO tetrahedrons. The lateral dimensions of the crystalline nuclei are of the same size as for cells on sputtered ZnO.

Then the crystallites grow almost perpendicular to the facets of LPCVD ZnO, forming large conglomerates, with lateral dimensions comparable to the lateral sizes of the ZnO tetrahedrons. In the first stage of growth these conglomerates are surrounded with amorphous material. When the coalescence of the conglomerates occurs, i.e., after 200–350 nm of growth [Figs. 2(c) and 2(d)], the heterophase layer ends depending on the height of the ZnO tetrahedrons. This makes the thickness of the heterophase layer $h$ a parameter, which is very sensitive to the topography of the TCO. For this reason we prefer to use as parameter the linear nuclei density $n_d$, in order to compare the cells grown on TCOs with different topographies. We have plotted in Fig. 5 the variation of $h$ and $n_d$ vs SC for cells deposited on sputtered ZnO and on LPCVD ZnO.

## IV. DISCUSSION

### A. Microstructure of $n-i-p$ cells

We have sketched the evolution of the microstructure of the *i* layer in solar cells deposited on flat sputtered ZnO in Figs. 7(a) and 7(b). These sketches suggest an analogy between the shape of the conglomerates and a pencil box.[17] Indeed, the conglomerates exhibit a cone-shaped end and a cylindrical or columnar body. Within this analogy, the tip of the pencil represents the nucleus of the first grain starting a conglomerate. The other grains then join the first grain and extend it vertically and laterally, forming the cone-shaped end of the conglomerate. The average opening angle of this cone as measured on the whole dilution series is $15° \pm 3°$ (with respect to the normal to the substrate). The conglomerates coalesce at the contact threshold, which corresponds to the thickness of the heterophase layer $h$. The analogy of the pencil box holds well for the sample deposited at SC=5% [Fig. 2(a)], whereas for the solar cell deposited at SC=7%

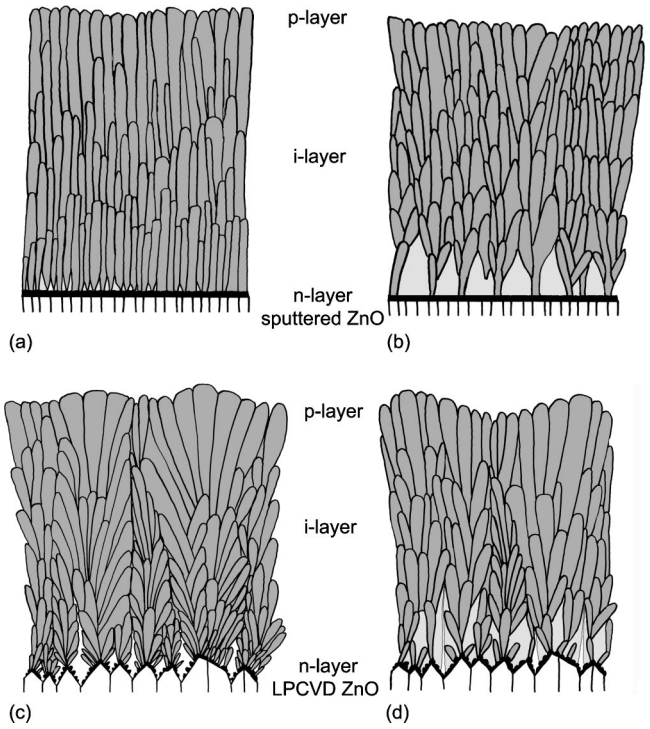


FIG. 7. Sketches of the microstructure evolution with respect to silane concentration (SC) for flat sputtered ZnO and rough LPCVD ZnO. These sketches are drawn from the original TEM micrographs given in Fig. 2. Dark gray regions represent crystalline material whereas light gray regions represent amorphous material. Voids/cracks are represented in white. The homogeneously thick *n*-layer on flat ZnO is represented with a black straight line on sketches (a) and (b). On the rough ZnO the *n* layer is not homogeneous any longer, it is, thus, represented by inhomogeneous black spots [sketches (c) and (d)]. One can see qualitatively how the heterophase layer is modified by the silane concentration SC on each of the two substrates used.

some competitive growth between the conglomerates above the heterophase layer can be observed [Fig. 2(b)], resulting in noncylindrical bodies of the pencils.

In Figs. 5(a) and 5(b), the inverse trend between $h$ and $n_d$ can be understood on sputtered ZnO by the observation of an almost constant opening angle $\alpha$ of the cone-shaped beginning of the conglomerates. From basic geometry, one can deduce the following relationship between the heterophase thickness $h$ and the nucleation density $n_d$:

$$n_d = 1/[2h\tan(\alpha)].$$

This simple relationship explains that $h$ and $n_d$ should, indeed, follow an inverse trend. In Fig. 5, this inverse trend is also observed for cells on LPCVD ZnO.

In Fig. 5(a), is also plotted the linear nuclei density for both types of substrate. Note that $n_d$ is, within a factor of two, lower on LPCVD ZnO than on sputtered ZnO. Whether this effect is due to the topography of the substrate or to the different *n* layer quality is still an open question.

Another characteristic of the microstructure of devices deposited on rough TCO is the growth direction of the crystallites: they start growing normal to the facet of the LPCVD ZnO tetrahedrons.[14,18] As growth proceeds, the direction of growth changes towards the normal of the average substrate plane. The ZnO tetrahedrons, thus, promote a starting fan-like growth of the conglomerates [see Figs. 7(c) and 7(d)].

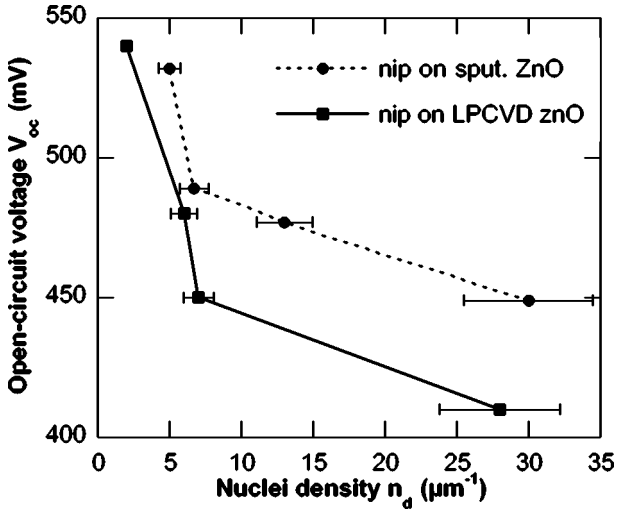


FIG. 8. Relationship between the linear density of nuclei $n_d$ and the open-circuit voltage $V_{oc}$ of the cells on sputtered and LPCVD ZnO. Note that $n_d$ is evaluated for the unfolded surface area of the underlying ZnO layer.

This fan-like type of growth is accompanied by competition between the conglomerates, resulting in an increasing lateral size of the conglomerates emerging at the surface of growth. Indeed, a conglomerate shadowing by its fan-like growth another conglomerate enhances its lateral size, whereas the lateral size of the covered conglomerate is reduced progressively to zero as the layer grows. As a consequence, a conglomerate starting on top of a higher-than-average tetrahedron will tend to win the competitive growth over the other conglomerates. The result of this process is that the highest tetrahedrons of the substrate are still perceptible on top of the cell, as observed in TEM micrographs in Figs. 2(c) and 2(d). This effect can partly explain the high value of surface roughness for cells deposited on LPCVD ZnO at high SC.

### B. Open-circuit voltage $V_{oc}$ of $n-i-p$ cells

As previously observed, increasing SC towards values close to the transition to amorphous material deposition conditions increases the value of $V_{oc}$. In this region of the space of deposition parameters, the changes in the microstructure of the *i* layer observed in this study, occur mostly in the heterophase layer. It is, thus, of interest to establish a relationship between the microstructural parameter $n_d$ and the value of $V_{oc}$.

In Fig. 8, we observe that the behavior of $V_{oc}$ vs $n_d$ exhibit the same trend on both substrates. The $V_{oc}$ established in cells on LPCVD ZnO is, however, lower than the cells on sputtered ZnO; this result could be due to the different outcome of the *n*-doped layers on the two substrates.

It is important to stress that we have not observed here that the amorphous phase simply constitutes a continuous amorphous incubation layer over the *n* layer. On the contrary, the amorphous phase is observed to surround the microcrystalline phase, insuring thus the passivation of the crystallite and/or conglomerate boundaries.

The lower that $n_d$ is, the larger that $h$ becomes [see Figs. 5(a) and 5(b)] and, consequently, the larger the average amorphous volume fraction is within the device. This effect is more pronounced on the rough substrate, where the valleys are filled with amorphous material and the thickness $h$ of the heterophase layer is consequently increased compared to the case of a flat substrate (see Fig. 5). Nevertheless, we have not been able here to quantify the microstructural changes above the heteorphase layer. Before attributing the observed variation of $V_{oc}$ with SC solely to the heterophase layer characteristics ($n_d$ and $h$) one should also look for any microstructural modifications of the material above the heterophase layer.

## V. CONCLUSIONS

Our detailed investigation of the material microstructure as incorporated in complete working $n-i-p$ devices shows that the silane concentration at which the $i$ layer is deposited has a major effect on the bottom of the $i$-layer microstructure, the so-called heterophase layer. Indeed, in these devices, the amorphous volume fraction is higher at the bottom of the i-layer. In particular, the crystalline nuclei density $n_d$ and the heterophase layer thickness $h$ vary notably with SC.

Furthermore, the substrate type (here flat sputtered ZnO and rough LPCVD ZnO, both on glass) influences the microstructure of the microcrystalline material: it affects the nature of the $n$ layer as well as the lateral sizes of the crystallite conglomerates and the roughness of the final device layer ($p$ layer). The latter plays an important role for the light scattering properties of the device.

For both series of $n-i-p$ cells a relationship between the microstructure (specifically, the linear nucleation density $n_d$) and the open-circuit voltage $V_{oc}$ of the devices has been presented: the lower the nucleation density the higher is the resulting value of $V_{oc}$. As a general consequence, technological control of the first stage of growth of the $i$ layer (i.e., of the heterophase layer) is of paramount importance to produce cells with a high value of $V_{oc}$.

## ACKNOWLEDGMENTS

The authors acknowledge the financial support from the Swiss Federal Office for Energy under Grant No. 38487 and the Swiss National Science Fund under Grant No. FN-59413.

[1] A. V. Shah, J. Meier, L. Feitknecht, E. Vallat-Sauvain, J. Bailat, U. Graf, S. Dubail, and C. Droz, Proceedings of the 17th EU Photovoltaic Solar Energy Conference, Münich, D, 2823 (2001).
[2] E. Vallat-Sauvain, U. Kroll, J. Meier, A. Shah, and J. Pohl, J. Appl. Phys. **87**, 3137 (2000).
[3] J. Meier *et al.*, Proceedings of the 2nd World Conference and Exhibition on Photovoltaic Solar Energy Conference, Vienna, Austria (1998), Vol. 1, p. 375.
[4] Y. Nasuno, M. Kondo, A. Matsuda, Sol. Energy Mater. Sol. Cells **74**, 497 (2002).
[5] S. Klein, F. Finger, R. Carius, B. Rech, L. Houben, M. Luysberg, and M. Stutzmann, Mater. Res. Soc. Symp. Proc. **715**, A26.2.1 (2002).
[6] J. Meier, E. Vallat-Sauvain, S. Dubail, U. Kroll, J. Dubail, S. Golay, L. Feitknecht, P. Torres, S. Fay, D. Fischer, and A. Shah, Sol. Energy Mater. Sol. Cells **66**, 73 (2001).
[7] O. Vetterl, F. Finger, R. Carius, P. Hapke, L. Houben, O. Kluth, A. Lambertz, A. Mück, B. Rech, and H. Wagner, Sol. Energy Mater. Sol. Cells **62**, 97 (2000).
[8] S. Guha, J, Yang, Y. Lubianiker, J. D. Cohen, and A. H. Mahan, Appl. Phys. Lett. **74**, 1860 (1999).
[9] M. Tzolov, F. Finger, R. Carius, and P. Hapke, J. Appl. Phys. **81**, 7376 (1997).
[10] J. Bailat, E. Vallat-Sauvain, L. Feitknecht, C. Droz, and A. Shah, J. Non-Cryst. Solids **299-302**, 1219 (2001)
[11] J. Koh, A. S. Ferlauto, P. I. Rovira, C. R. Wronski, and R. W. Collins, Appl. Phys. Lett. **75**, 2286 (1999).
[12] J. Benedict, R. Andersen, and S. J. Klepeis, Mater. Res. Soc. Symp. Proc. **254**, 121 (1992).
[13] A. Poruba, A. Fejfar, Z. Remes, J. Springer, M. Vanecek, J. Kocka, J. Meier, P. Torres, and A. Shah, J. Appl. Phys. **88**, 148 (2000).
[14] J. Dubail, E. Vallat-Sauvain, J. Meier, S. Dubail, and A. Shah, Mater. Res. Soc. Symp. Proc. **609**, A13.6.1 (2001).
[15] M. Luysberg, C. Scholten, L. Houben, R. Carius, F. Finger, and O. Vetterln, Mater. Res. Soc. Symp. Proc. **664**, A15.2.1 (2001).
[16] E. Vallat-Sauvain, S. U. Kroll, J. Meier, and J. A. Shah, Mater. Res. Soc. Symp. Proc. **664**, A15.3.1 (2001)
[17] A. Fejfar, T. Mates, C. Koch, B. Rezek, V. Svrcek, P. Fojtik, H. Stuchlikova, J. Stuchlik, and J. Kocka, Mater. Res. Soc. Symp. Proc. **664**, A16.1.1 (2001).
[18] Y. Nasuno, M. Kondo, and A. Matsuda, Mater. Res. Soc. Symp. Proc. **664**, A15.5.1 (2001).